COBEM 2023 27TH INTERNATIONAL CONGRESS OF MECHANICAL ENGINEERING

ABCM Brazilian Society of Mechanical Sciences and Engineering
27th ABCM International Congress of Mechanical Engineering
December 04-08, 2023, Florianópolis-SC, Brazil

COB-2023-2374
MODELING AND SIMULATION OF THERMAL EFFECTS IN CYLINDRICAL PLUNGE DRY GRINDING WITH PRECOOLING

Ézio Carvalho de Santana
Gabriel Urbano de Souza
Eraldo Janonne da Silva
University of São Paulo, São Carlos School of Engineering, Av. Trab. São Carlense, 400 - Parque Arnold Schimidt, 13566-590, São Carlos, SP, Brazil.
eziocds@usp.br, gabriel.urbano.souza@usp.br, eraldodasilva@usp.br.

Daniel Weber
Benjamin Kirsch
Jan Christian Aurich
Institute for Manufacturing Technology and Production Systems, RPTU in Kaiserslautern, Gottlieb-Daimler-Str., 67663 Kaiserslautern, Germany.
daniel.weber@rptu.de, benjamin.kirsch@rptu.de, fbk@mv.rptu.de.

Abstract. *In grinding operations, metal working fluids (MWF) are used to minimize heat-associated problems such as surface cracks, burning, and tensile residual stresses. Filtration, recycling, and disposal of MWFs are additional cost factors. As a means to eliminate the use of MWFs, a method of dry grinding was developed with precooled parts. In this method, a cryogenic medium is used to precool the part and subject it to grinding operation without any MWF supply. However, the performance of the precooled parts in dry grinding depends on the shape, size, and dimensions of the part. For this matter, it is useful and economical to perform thermal simulations in order to predict the effectiveness of precooling. Therefore, Finite Element Analysis (FEA) simulations were employed to model grinding as a moving heat source to evaluate maximum temperatures on cylindrical workpieces. The numerical cylindrical plunge grinding simulations were then validated by dry grinding experiments with and without precooling being applied and an excellent agreement was found between the simulation's predictions and experimental measurements of temperature.*

Keywords: *Cylindrical plunge grinding, Thermal Simulation, Cryogeny, Precooling, Finite Element Method.*

1. INTRODUCTION

As a finishing manufacturing process, grinding is highly dependent on the workpiece's temperature, and the manner in which this temperature varies throughout the process should be properly understood in order to prevent any form of distortion on the final product's geometry. To avoid excessive temperatures, metal working fluids (MWFs) — a mixture of water and oil — are widely employed in the industry. As MWFs are costly and environmentally negative, cryogenic fluids are a possible alternative to dissipate the heat generated in the process.

Regarding cryogenic cooling, it is a choice whether to employ active liquid nitrogen pressured jet cooling or precooling. Precooling stands for simply cooling down the workpiece by submerging it in cryogenic fluid such as liquid nitrogen or carbon dioxide, or any other methods, to achieve a desired low temperature before the grinding operation takes place. Such procedure has been tested by Oliveira et al. (2015), where it was proposed that the workpiece's dimensions, more specifically its volume over surface area ratio V/A_s, will heavily impact the precooling's effectiveness. Instead of performing multiple experiments on workpieces with different sizes, a much more economical solution consists in developing a thermal model to evaluate peak surface temperature reached numerically. Weber et al. (2023) have already validated thermal simulations for surface grinding of precooled parts in a similar manner to the procedure adopted in this work. Sakakura et al. (2012) pointed out that due to the technical difficulties in performing temperature measurements on a rotating workpiece, the development and validation of plunge cylindrical grinding simulations has not received sufficient attention. In their work, Sakakura et al. (2012) proposed and validated a thermal model for wet grinding considering an intensified heat loss from the workpiece to the cutting fluid through a convection model, and a localized heat flux on the workpiece's surface, representing a fraction of the heat produced in the grinding zone, with its magnitude being determined by the mean value of tangential force measurements. Nonetheless, numerical simulations for dry cylindrical plunge grinding continue to be scarce among the current literature and may be useful for other ends besides evaluating the precooling strategy. Thus, this work aims to develop and experimentally validate numerical simulations of dry plunge grinding with or without precooling.

2. DEVELOPMENT

This section is divided in the 'Modeling and simulation set-up' subsection, which contains all the information related to the modeling of the thermal phenomena in a cylindrical plunge grinding process and the implementation of these models as boundary conditions in the simulations; the 'Grinding experiments' subsection, which contains information of the dry grinding and precooling experiments conducted; and the 'Numerical validation' subsection, which contains the comparison between numerical simulations and experimental results.

2.1 Modeling and simulation set-up

To set up the grinding simulations, it is first necessary to break down thermal interactions happening during the process. Regarding the thermal model employed, heat exchange in a grinding process occurs according to three main phenomena, as shown in Figure 1.

Firstly, there is convective heat transfer Q_{conv} to air, which is modeled by Eq. (1), where h [W/(m²ºC)] is the convection coefficient, T_{amb} [ºC] is the ambient temperature and T [ºC] is the temperature of the node subjected to this boundary condition. All external nodes of the workpiece's mesh are subjected to this boundary condition.

$$Q_{conv} = h\,(T_{amb} - T) \tag{1}$$

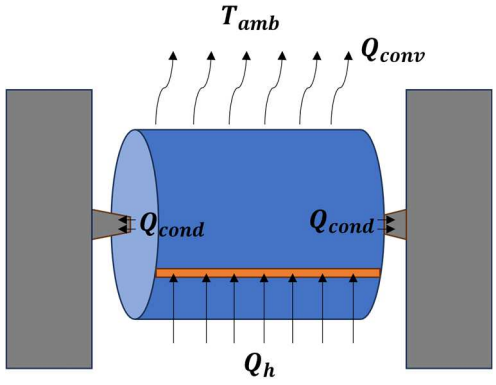

Figure 1. Schematic diagram of the boundary conditions.

Secondly, the heat transfer by thermal contact conductance Q_{cond} occurs at the contact region between workpiece and center supports. Thus, the center supports have been 3D-modeled and added to the finite element method (FEM) assembly. The thermal contact conductance was modeled by Eq. (2) and assigned as boundary condition for all the nodes of the workpiece and center supports in contact with each other. The parameter k_c [W/(m²ºC)] is the contact conductance coefficient, T_a [ºC] is the temperature of the workpiece's node and T_b [ºC] is the temperature of the center support's node which share this interaction.

$$Q_{cond} = k_c\,(T_a - T_b) \tag{2}$$

In order to determine the convective coefficient h and contact conductance coefficient k_c of the previous boundary conditions, four experiments were conducted, as listed in Table 1. Experiments 1 and 2 consisted in heating a workpiece to the boiling point of water and then allowing it to cool naturally in air (natural convection only) or while clamped by the center supports in the grinding machine (convection combined with conductance). Experiments 3 and 4 followed a similar procedure, but instead the workpiece is cooled in liquid nitrogen and allowed to heat naturally in air or while clamped in the machine.

Table 1. Convection and conductance experiments.

Experiment #	Initial temperature (°C)	Convection	Conductance (contact)
1	100	✓	✗
2	100	✓	✓
3	-196	✓	✗
4	-196	✓	✓

Lastly, the heat generated in the grinding zone Q_h is modeled as a moving heat flux, which is applied evenly to the grinding zone, rotating around the cylinder according to the workpiece's rotational frequency N_w [rpm]. The movement the heat flux performs is illustrated by the temperature maps at different instances in Figure 2(a) and Figure 2(b). In ABAQUS, a DFLUX subroutine is necessary to implement this moving heat source, as it allows the user to define where the heat source is located, its area and the magnitude of the heat flux.

The heat load is defined as surface-based heat flux and is applied to the arc area delimited by the points P1, P2, P3 and P4 in Figure 3. The angular position θ [°] is a function of time t [s] and rotational frequency of the workpiece in the grinding experiment N_w [rpm] (Eq. (3)), and α [°] is a function of the geometric contact length l_c [m] in Eq. (5) (Rowe et al., 1993) and function of the cylinder's radius r [m] (Eq. (4)). In the longitudinal direction of the cylinder, the heat flux is applied throughout its whole length.

$$\theta = \frac{360°}{60} N_w t \tag{3}$$

$$\alpha = \frac{l_c}{r} \frac{180°}{\pi} \tag{4}$$

$$l_c = \sqrt{a_e d_e} \tag{5}$$

Where a_e is the depth of cut and d_e is the grinding wheel's equivalent diameter, given by Eq. (6) (Qi et al., 1997), d_s is the grinding wheel diameter, and d_w is the workpiece diameter.

$$\frac{1}{d_e} = \frac{1}{d_s} + \frac{1}{d_w} \tag{6}$$

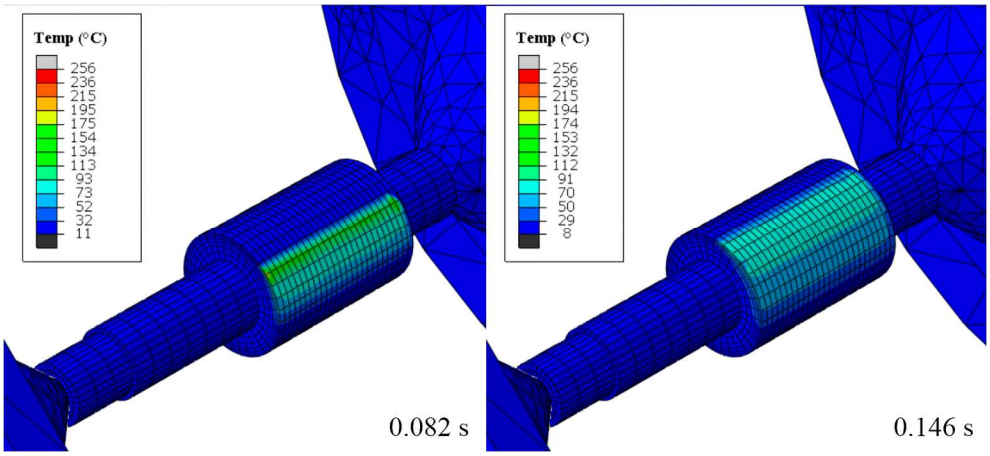

(a) (b)

Figure 2. Temperature field maps of the workpiece at different instances to depict the movement of the heat flux.

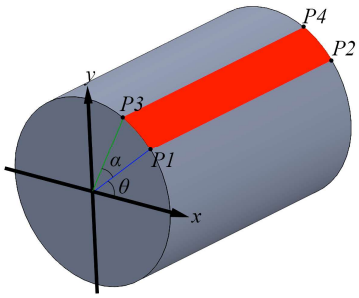

Figure 3. Position and area schematics of the moving heat flux.

The magnitude of the heat flux is computed using the experimental grinding power data measured by the grinding machine system as an input. The variation in electric power consumption while the grinding process is ongoing P [W] is used to calculate specific heat flux q_w [W/m²] according to Eq. (7) (Malkin and Guo, 2007), where b is the grinding width [m] and R_w is the energy partition to the workpiece.

$$q_w = \frac{R_w\, P}{l_c\, b} \tag{7}$$

The precooling can be implemented in the simulations through a simple Dirichlet boundary condition, which essentially sets the initial temperature of all the workpiece's nodes. The thermal modeling and boundary conditions applied in this work are already validated for surface grinding in Weber et al. (2023).

Two 3D models of the workpieces were elaborated for the thermal simulations based on its experimental counterparts, which will be introduced in the next subsection. Regarding the model's meshes, an average distance value between the nodes of the model's elements of 1.5 mm was used to generate the mesh of the smaller workpiece's model (WP D28), while an average distance value of 5 mm was used on the larger workpiece's model (WP D100), to reduce processing time. In both cases, near-surface elements were kept at no more than 1 mm size. Elements must be set to "Coupled temperature-displacement" type, and were left as Standard element library and linear geometric order. The D28 assembly mesh features 14633 nodes and 14816 elements on the workpiece and 986 nodes and 3691 elements at each of the center supports. On the other hand, the D100 assembly mesh features 6888 nodes and 5920 elements at the workpiece and the same number regarding its center supports. A view cut of both model's meshes can be seen in Figure 4.

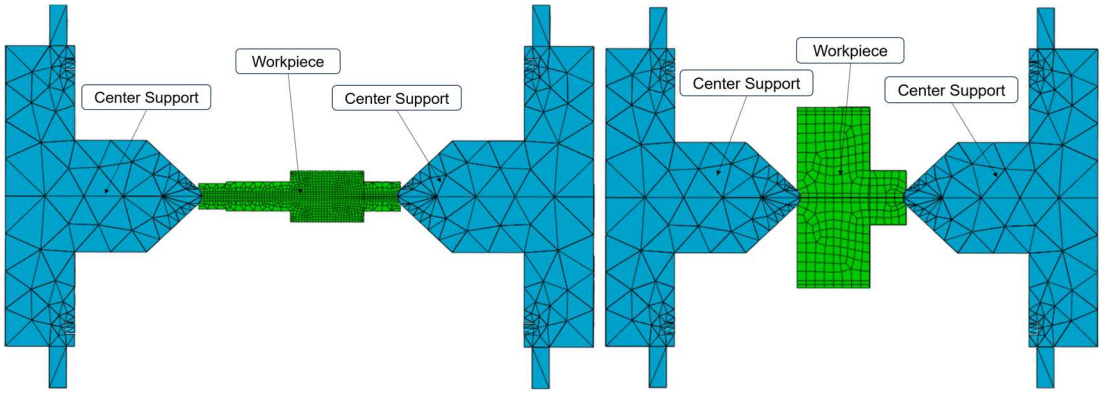

(a) (b)

Figure 4. D28 (a) and D100 (b) simulation assemblies and visualization of internal mesh through a view cut.

2.2 Grinding experiments

The ground workpieces were made from a steel SAE 4140 billet. These workpieces were quenched and tempered until a superficial hardness value of 58 HRC was reached. The workpiece's physical properties and geometrical dimensions are presented in Table 2 and Figure 5.

Table 2. Thermal and physical properties of the AISI 4140 steel workpiece.

Physical property	**Value**
Thermal conductivity [W/(m.°C)]	42.6
Density [kg/m³]	7850
Specific heat [J/(kg.°C)]	486

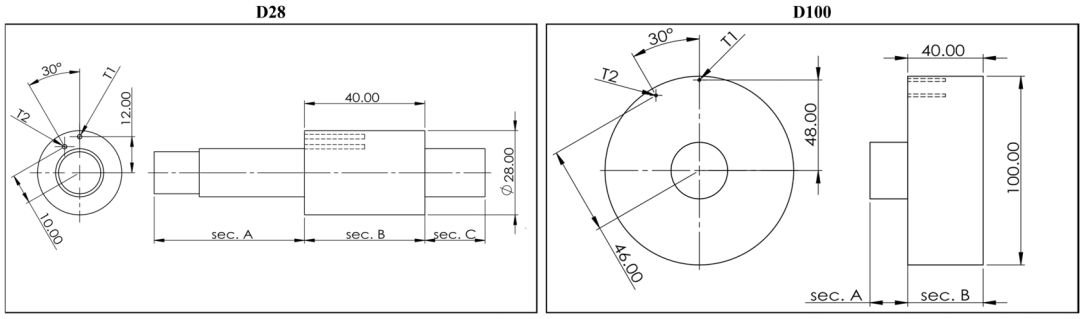

(a) (b)

Figure 5. Workpiece's D28 and D100 dimensions.

For the temperature measurement during the grinding process, two type K thermocouples were inserted in the specimen's blind holes T1 and T2 (see Figure 5). The hole farthest from the center of the cylinder, located at a distance of 2 mm from the outer surface of section B of the part, was referred to as T1; whereas the innermost point, located at a distance of 4 mm from the outer surface, was referred to as T2. The thermocouples were inserted into these cavities until the tip of each thermocouple touched the end of the blind holes.

For a cylindrical plunge grinding process, temperature measurements using thermocouples connected to a stationary data processing unit would result in the wires getting entangled due to the workpiece's rotation. Therefore, a signal emission device that rotates accompanying the workpiece's movement was used. This device transmits the thermocouple signals via Bluetooth to an external receiving unit connected to the NI USB-6341 device. The NI-USB-6341 device then sends these signals to a laptop for data visualization, processing and extraction purposes. This measurement setup is shown in Figure 6.

The temperature measurement system produces digital signals at a sample rate of 500 Hz with 12 bits of resolution. Regarding the post-processing of the data, a moving average filter with window length of 61 elements was employed to reduce the signal's noise.

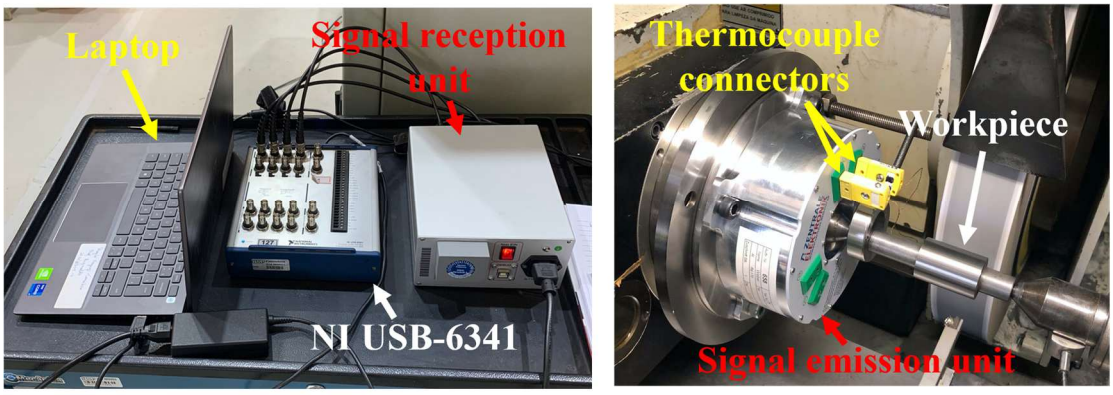

Figure 6. Experimental temperature measurement system.

Two grinding experiments were conducted in this work for validation's purpose, one dry grinding experiment without precooling and the other with precooling. For the dry griding experiment without precooling, the D28 workpiece (Figure 5(a)) was used; while for the precooling experiment the D100 workpiece (Figure 5(b)) was used instead, since it has more volume than the D28 and therefore more thermal inertia, making the experiment easier to execute. The following grinding parameters were adopted for the validation's experiments: 30 m/s cutting speed, workpiece's rotational frequency N_w of 100 rpm, stock removal from the workpiece's diameter of 0.3 mm and 6.7 s of spark out time. A specific material removal rate of 0.83 mm³/(mm.s) was maintained for both experiments, meaning the D28 workpiece (Figure 5(a)) will be subjected to an infeed rate v_f of 0.566 mm/min and depth of cut per revolution a_e of 5.66 µm, while the D100 (Figure 5(b)) will present v_f and a_e values of 0.159 mm/min and 1.59 µm. An aluminum oxide grinding wheel with diameter of 500 mm (38 A 80 J VHB) was used in the experiments. The dressing of the wheel was performed adopting an overlap ratio U_d of 7.

The power consumption during the grinding experiments was measured from the SINAMICS G120 - CU320 control, from Siemens AG, where the electric power data was transmitted via crossover cable to a PC and then collected using the STARTER software, also from Siemens AG. A moving average filter with window length of 61 elements was also applied to the power measurements collected data in order reduce the signal's noise

2.3 Numerical Validation

This section presents the comparisons between numerical simulations and experimental data for the convection and conductance experiments, and the dry grinding experiments with and without precooling.

2.3.1 Convection and Conductance

Early simulations focused solely on heat exchange from convection with or without conductance, in order to determine the convection coefficient h and the contact conductance coefficient k_c to be used in the simulations. These coefficients were iteratively refined through a systematic process of parameter optimization, guided by the objective of matching the experimental results, known commonly as the inverse method. The agreement between numerical and experimental curves observed in Figure 7 was attained at the end of this iterative process using the h and k_c values presented in Table 3.

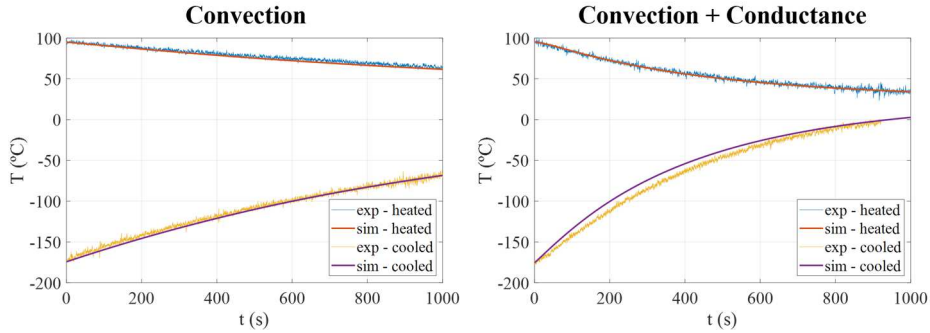

Figure 7. Simulation results for convection and conductance estimated effects compared to experimental data.

Table 3. Convection and conductance coefficient values used for simulations.

T [ºC]	h [W/(m².ºC)]	h_c [W/(m².ºC)]
< -170	14	
-140	14	
-110	14	
-50	12	
0	10	9000
40	8	
80	10	
120	12	
140	14	

2.3.2 Moving Heat Source

The dry grinding experiment of the D28 workpiece, as mentioned in subsection 2.2, was performed with an infeed rate of 0.566 mm/min, stock removal from its diameter of 0.3 mm and spark-out of 6.7 s. Considering these parameters, the expected process time would be a spark-in of 15.9 s and spark-out of 6.7 s, totaling 22.6 seconds. However, examining the acoustic emission map in Figure 8, the contact between grinding wheel and workpiece was not uniform throughout the process.

The acoustic map represents the distribution of acoustic emission in the contact region between grinding wheel and workpiece over time, in RMS voltage, according to the method developed by Oliveira and Dornfeld (1994, 2001). The acoustic map graph contains the value of the acoustic emission (AE) signal captured by an AE sensor positioned next to the grinding wheel. This AE signal, after processing, is plotted on a color scale ranging from 0 (no contact) to 3 U_{rms} (maximum intensity), which can be correlated with the intensity of contact between the grinding wheel and the surface of the workpiece being machined. The vertical axis of the map corresponds to the discretization of the grinding wheel profile with respect to the angular position of the proximity sensor. On the other hand, the horizontal axis indicates the number of revolutions of the grinding wheel performed during one grinding cycle. At the beginning and end of the grinding cycle (vertical lines near 0 and 300 revolutions in Figure 8, respectively), vertical lines with irregularities in the U_{rms} intensity values were detected, with sections delimited by red arrows, demonstrating the non-uniform nature of the contact between workpiece and grinding wheel.

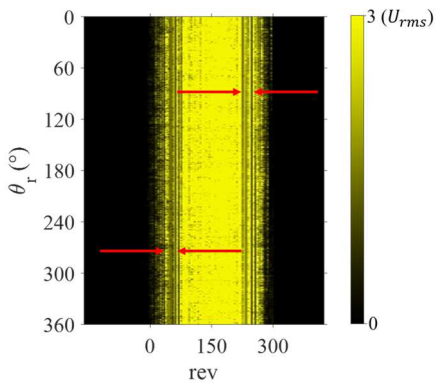

Figure 8. Dry grinding acoustic map.

The final diameter of the workpiece after the grinding process was 27.763 mm, meaning the determined stock removal value of 0.3 mm was not fully achieved. Considering the volume of material removed from the workpiece and assuming a constant infeed rate of 0.566 mm/min, it was estimated that 12.6 seconds was a more suitable value to describe the actual process time from beginning until completion of the machining process. Therefore, a process time of 12.6 s was adopted for the simulation's execution, meaning the moving heat source should perform 21 revolutions around the workpiece, since $N_w = 100\ RPM$.

The average grinding power during the grinding cycle (interval between 15 and 38 seconds in Figure 9(a)) of 1393.67 W was subtracted by the base power value of the machine while no grinding is taking place (538.88 W). For simplicity's sake, an average power value of 855 W was adopted. The grinding width was 40 mm, which is equal to the length of the D28 workpiece's sec. B (see Figure 5 (a)) and the energy partition to the workpiece R_w for the computation of the moving heat source's magnitude was 0.7, being a reasonable value considering it is between the 0.7 and 0.8 range proposed by García et al. (2014). Lastly, the geometric contact length can be computed according to Eq. (5) as a function of depth of cut (5.66 µm), workpiece diameter (28 mm) and grinding wheel diameter (500 mm) and presents a value of 0.38 mm. The magnitude of the moving heat source was considered uniform and a constant value of $\bar{q}_w = 38.62$ MW/m² was computed based on Eq. (7). The initial temperature value was set to 25 °C for all nodes in the simulation.

With all the boundary conditions fully defined, the simulation was executed and the numerical temperature values at points T1 and T2 were compared with the experimental measurements, which can be seen in Figure 9 (b,c). The observed slope difference between the curves at the start and end of the grinding can be justified by the usage of an average grinding power value in simulations, while experimentally there is a clear non uniformity in contact between workpiece and grinding wheel, as mentioned previously, and therefore the power consumption during the process is not constant. Nonetheless, the agreement found between the curves is remarkable, with numerical peak values for T1 and T2 of 187.02 and 177.83 ºC, and experimental peak values of 204.47 and 184.89 ºC, respectively. The relatively small difference between numerical and experimental values can be explained by the model's simplifications, such as assuming an uniform heat flux along the length of the grinding, and also the uncertainty of the experimental measurements.

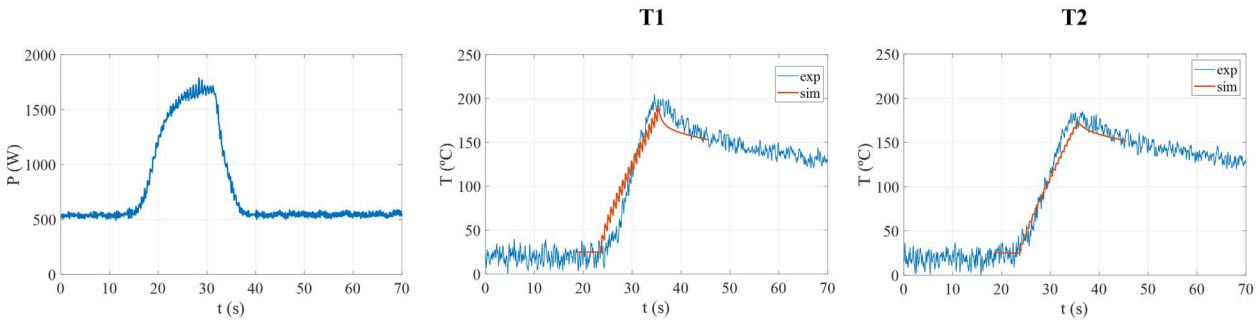

Figure 9. Dry grinding experimental power curve (a) and comparison between simulation's predicted temperature values for points T1 and T2 (in orange) and experimental measurements (in blue) using the D28 workpiece.

2.3.3 Precooling Boundary Condition

The precooling experiment and simulation were executed in a similar manner to the dry grinding procedure, however there are a few key differences. As mentioned in section 2.2, the ground workpiece was the D100 instead, and the manner by which q_w is calculated was modified. In the dry grinding simulation, an average value was computed from the experimental power curve in Figure 9(a). For the precooling simulation on the other hand, it was necessary to consider the variation of the process' power consumption as a function of time due to two main reasons.

First, the contraction of the workpiece after the precooling led to an extremely non-uniform contact between the workpiece and grinding wheel, which can be observed in Figure 10. The progression of contact during grinding at 26, 37, 42, and 59 seconds can be observed through the gradual disappearance of the ice layer on the workpiece ('B' element in Figure 10) and the uneven adherence of the removed material to the grinding wheel ('A' element in Figure 10), causing a localized darkening. This lack of contact produces a power curve which increases very gradually until reaching its peak just before the end of the cycle, as shown in Figure 11(a). A non-uniform contact between workpiece and grinding wheel also occurred in the dry grinding experiment from the previous subsection, but not to this extent.

Second, since the specific material removal rate was the same for both grinding experiments conducted in this study, but the diameter of the workpiece was increased for the precooling process, the infeed rate had to be decreased to a value of 0.159 mm/min, resulting in a spark-in time interval of 56.6 seconds. This long process time meant that while the temperature near the surface of the workpiece increases as a product of the heat generated during grinding, this rate of change in temperature is decreased by the precooled interior of the workpiece, which absorbs a significant part of this heat, reducing the rise in temperature near the surface of the workpiece. This aspect can be seen in Figure 11(b,c), where

after the end of the grinding process (approximately 63 s), both measured and numerical temperatures drop rather than continuing to approach ambient temperature. If instead an average power consumption value and average process time were used, this dynamic heat exchange between the precooled interior of the material and its heated surface would not be well represented, since its effect accumulates over time, being more significant as the process' time increases.

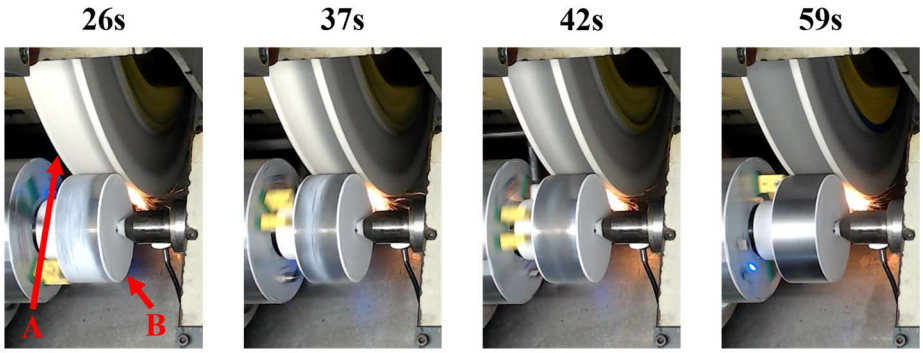

Figure 10. Different frames from the video capture of the grinding process with precooling.

Given the depth of cut (1.59 µm) and workpiece diameter (100 mm) were different from the dry grinding experiment previously described, the geometric contact length l_c had to be recalculated and assumed a value of 0.36 mm. The grinding width b and energy partition R_w to the workpiece on the other hand remained the same.

In order to compute $q_w(t)$, the power $P(t)$ input in Eq. (7) was fitted by a sum of exponential functions, aiming to filter the signal's noise. The power curve which the fit was applied to can be observed in Figure 11 (a). The precooling boundary condition was implemented by defining the initial temperature value of all the workpiece's nodes to -115 °C, which was the measured temperature of the workpiece at the beginning of the grinding process, while the nodes belonging to center supports start at room temperature (25 ºC).

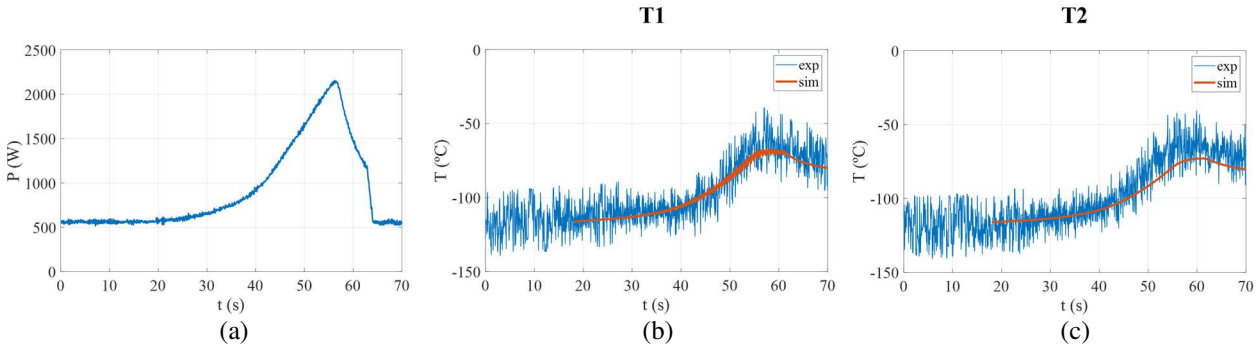

Figure 11. Dry grinding with precooling experimental power curve (a) and comparison between simulation's predicted temperature values for points T1 and T2 (in orange) and experimental measurements (in blue).

The simulation results with precooling also achieved a high degree of accordance in comparison to the experimental data, as seen in Figure 11(b,c), with peak values of temperature for T1 and T2 of -67.65 and -72.93 from the simulations and -39.31 and -40.74 from experimental measurements. The peak temperature values are not as close when compared to the dry grinding numerical and experimental comparison in the previous subsection, but they still show a good overall agreement considering the noise present in the temperature measurements elevate considerably the experimental peak value registered. Furthermore, employing a moving heat source with its magnitude dependent on time significantly improved the shape of the numerical curve, better matching the observed temperature behavior of points T1 and T2 in the experiments. The results presented demonstrate the good quality of the models and simulations developed in this work.

3. CONCLUSIONS

The research conducted managed to develop cylindrical plunge grind simulations presenting remarkable accuracy while maintaining certain simplicity with respect to the thermal modeling. Convection and conduction effects were modeled by inverse method, while the moving thermal source was implemented based on experimental power measurements. Finally, a Dirichlet condition was employed to represent the precooling of the workpiece in the

simulations. Future steps of this research include the development of models to predict power consumption during the process in order to reduce the dependency of the simulations on experimental measurements, the inclusion of in-process cryogenic cooling boundary condition in the simulations, and a study of mesh convergence to improve computational efficiency.

4. ACKNOWLEDGEMENTS

The authors would like to thank the Conselho Nacional de Desenvolvimento Científico e Tecnológico (CNPq) and the Fundação de Amparo à Pesquisa do Estado de São Paulo (FAPESP) for their financial support of the project "Expanding the Possibilities of Cryogenic Assisted Grinding" (FAPESP Grant No. 2018/16416-5) and Deutsche Forschungsgemeinschaft DFG with DFG-project number 440394762.

5. REFERENCES

García, E., Méresse, D., Pombo, I., Harmand, S., Sánchez, J.A., 2014, Identification of heat partition in grinding related to process parameters, using the inverse heat flux conduction model, Applied Thermal Engineering, Vol. 66, n. 1, pp. 122–130, ISSN 1359-4311.

Malkin, S., Guo, C., 2007, Thermal analysis of grinding, CIRP Annals, Vol. 56, n. 2, pp.760–782, ISSN 0007-8506.

Oliveira, J.F.G., Dornfeld, D.A, 1994, Dimensional characterization of grinding wheel surface through acoustic emission, CIRP Annals, Vol. 43, n. 1, pp. 291–294, ISSN 0007-8506.

Oliveira, J.F.G., Dornfeld, D.A., 2001, Application of ae contact sensing in reliable grinding monitoring, CIRP Annals, Vol. 50, n. 1, pp. 217–220, ISSN 0007-8506.

Oliveira J.F.G., Silva, E.J., Coelho R.T., Brozek, L., Bottene, A.C., Marcos, G.P., 2015, Dry grinding process with workpiece precooling, CIRP Annals, Vol. 64, n. 1, pp. 329–332, ISSN 0007-8506.

Qi, H.S., Rowe, W.B., Mills, B., 1997, Contact length in grinding part 2: Evaluation of contact length models, Proceedings of the Institution of Mechanical Engineers, Part J: Journal of Engineering Tribology, Professional Engineering Publishing, Vol. 211, pp. 77–85, ISSN 13506501.

Rowe, W.B., Morgan, M.N., Qi, H.S., Zheng, H.W., 1993, The effect of deformation on the contact area in grinding, CIRP Annals, Vol. 42, n. 1, pp. 409–412, ISSN 0007-8506.

Sakakura, M., Ohnishi, T., Shinoda, T., Ohashi K., Tsukamoto, S., Inasaki, I., 2012, Temperature distribution in a workpiece during cylindrical plunge grinding, Production Engineering Research and Development, Vol. 6, n. 2, pp. 149–155, ISSN 1863-7353.

Weber, D., Kirsch, B., Silva, J.S., Silva, E.J., Aurich, J.C., 2023, 3D FEM heat transfer simulation of surface grinding of cryogenic pre-cooled parts, Procedia CIRP, Vol. 117, pp. 205–210, ISSN 2212-8271.

6. RESPONSIBILITY NOTICE

The authors are the only responsible for the printed material included in this paper.